QUANTIFICATION OF INLET IMPEDANCE CONCEPT AND A STUDY OF THE RAYLEIGH FORMULA FOR NOISE RADIATION FROM DUCTED FAN ENGINES

Joe W. Posey*
NASA Langley Research Center, Hampton, Virginia

M. H. Dunn†
Old Dominion University, Norfolk, Virginia

F. Farassat‡
NASA Langley Research Center, Hampton, Virginia

Presented at the 4th AIAA/CEAS Aeroacoustics Conference
June 2-4, 1998, Toulouse, France

Abstract

This paper addresses two aspects of duct propagation and radiation which can contribute to more efficient fan noise predictions. First, we assess the effectiveness of Rayleigh's formula as a ducted fan noise prediction tool. This classical result which predicts the sound produced by a piston in a flanged duct is expanded to include the uniform axial inflow case. Radiation patterns using Rayleigh's formula with single radial mode input are compared to those obtained from the more precise ducted fan noise prediction code TBIEM3D. Agreement between the two methods is excellent in the peak noise regions both forward and aft. Next, we use TBIEM3D to calculate generalized radiation impedances and power transmission coefficients. These quantities are computed for a wide range of operating parameters. Results were obtained for higher Mach numbers, frequencies, and circumferential mode orders than have been previously published. Viewed as functions of frequency, calculated trends in lower order inlet impedances and power transmission coefficients are in agreement with known results. The relationships are more oscillatory for higher order modes and higher Mach numbers.

*Senior Research Engineer, Member
†Associate Professor, AIAA Member
‡Senior Research Scientist, AIAA Associate Fellow

List of Symbols

Dimensional quantities are denoted by a tilde (~)

$\tilde{c}$	Ambient speed of sound
I_z^m	Axial component of acoustic intensity for *m-th* circumferential mode
J_m	*m-th* order Bessel function of the first kind
k	$=\begin{cases}\frac{m\tilde{r}_D\tilde{\Omega}}{\tilde{c}} & m\neq 0\\ \frac{\tilde{r}_D\tilde{\Omega}}{\tilde{c}} & m=0\end{cases}$ Nondimensional characteristic wavenumber
m	$=0,\pm1,\pm2,\ldots$ Circumferential mode number
M	Inflow Mach number
n	Radial mode number
$\tilde{r}_D$	Duct radius
t	Time
p'	acoustic pressure in ground fixed frame
P^m	*m-th* modal coefficient of acoustic pressure in duct fixed frame
(r,ψ,Z)	Cylindrical coordinates in duct fixed frame
U_z^m	*m-th* modal coefficient of axial component of acoustic velocity in duct fixed frame
v_n	normal component of acoustic velocity in ground fixed frame
β	$=\sqrt{1-M^2}$ Compressibility (stretching) parameter
κ	$=\frac{k}{\beta}$ Stretched characteristic wavenumber
κ_{mn}	$=\frac{1}{\beta}\sqrt{\kappa^2-\nu_{mn}^2}$ Axial wavenumber

ν_{mn} *n-th* zero of J'_m, $n = 0,1,\ldots$ for $m = 0$ and $n = 1,2,\ldots$ for $m \neq 0$

Π_n^m Power transmission coefficient for *m-th* circumferential mode and *n-th* radial mode

$\tilde{\rho}_0$ Ambient density

ζ_{nl}^m Generalized radiation impedance for *m-th* circumferential mode due to interaction of *n-th* radial pressure mode with *l-th* radial velocity mode

$\tilde{\Omega}$ Temporal frequency (radians/second)

Introduction

Today's civil jet transport aircraft are about 20 dB quieter than were those introduced some 40 years ago. Aircraft became quieter as turbojets were replaced by turbofans, sound-absorbing liners were added to the inlet and exhaust ducts, inlet guide vanes were eliminated, and bypass ratios grew larger. Still, airport communities around the world would like to see even less noisy aircraft.

As bypass ratios have increased, average exhaust velocities have decreased, resulting in less jet noise. At the same time, fan noise has increased because more of the thrust comes from the fan.

This paper addresses two aspects of duct propagation and radiation which can contribute to more efficient fan noise predictions, facilitating parametric screening and trend studies. In both cases, we use the ducted fan noise prediction computer program TBIEM3D[1]. The code, based on a boundary integral equation method (BIEM)[2], calculates the acoustic pressure anywhere in the sound field due to the scattering of incident sound by a finite length, cylindrical duct in a uniform flow field. The duct walls can be hard or lined and incident sound is generated by simple point sources.

First, we assess the effectiveness of Rayleigh's formula as a ducted fan noise prediction tool. The formula gives the acoustic pressure field due to a piston in a rigid wall and requires the acoustic pressure or the normal component of velocity on the piston as input. For the no inflow case and when only one propagating mode is present the formula is simple to implement and has been applied to inlet radiation problems by many researchers.

In this paper, we extend the formula to include the uniform axial inflow case. Noise radiation results using Rayleigh's formula with single propagating mode input are compared with TBIEM3D calculations.

Next, we use TBIEM3D to calculate generalized radiation impedances and power transmission coefficients. When a propagating spinning mode in a duct reaches the inlet, part of the energy is radiated and part reflected due to the abrupt change in geometry. The process is complicated by edge diffraction. TBIEM3D accounts for these phenomena. Previous researchers have relied on less exact noise prediction methods[3-8] for impedance calculations. Comparisons with these works are discussed.

Generalized radiation impedances and power transmission coefficients provide important noise radiation characteristics to the engine designer. We demonstrate the usefulness and versatility of TBIEM3D as a design tool by calculating these parameters for a wide range of operating parameters and circumferential mode numbers.

Part I: Rayleigh's Formula

Theory

In the analysis that follows all variables have been nondimensionalized: length by $\tilde{r}_D$, mass by $\tilde{\rho}_0 \tilde{r}_D^3$, and time by $\tilde{r}_D \tilde{c}^{-1}$.

Rayleigh's formula gives the acoustic pressure field due to a vibrating piston in a rigid wall[9]. Tyler and Sofrin, in their classical work on duct propagation and radiation, proposed the formula for calculation of the acoustic radiation field due to propagating modes from a semi-infinite, flanged duct with no flow[10].

The application of Rayleigh's formula to inlet (or exhaust) radiation requires knowledge of either the normal component of acoustic velocity or the acoustic pressure on the inlet (or exhaust) surface. It is assumed that these quantities are zero everywhere else on the plane containing the inlet (or exhaust). Furthermore, the acoustic pressure is assumed to be zero in the region of space behind the inlet disc if inlet radiation is considered or in front of the exhaust disc if exhaust radiation is desired.

We briefly derive a version of Rayleigh's formula that is valid with or without flow. Consider the radiation of sound from the inlet of an infinitesimally thin, hard walled, finite length, cylindrical duct in the presence of a uniform axial inflow. We adopt the usual spinning mode representation and assume that the *m-th* circumferential mode of acoustic pressure has the form

$$p^m(r,\psi,Z,t) = P^m(r,Z)e^{i\left(kt - m\psi - \frac{\kappa M}{\beta}Z\right)}. \qquad (1)$$

It is shown in reference 2 that the modal coefficient P^m is a solution of the two-dimensional Helmholtz equation

$$\left[\frac{1}{r}\frac{\partial}{\partial r}\left(r\frac{\partial}{\partial r}\right)+\frac{\partial^2}{\partial^2\xi}-\frac{m^2}{r^2}+\kappa^2\right]P^m(r,\xi)=0\,, \quad (2)$$

where

$$\xi=\frac{Z}{\beta} \quad . \quad (3)$$

The free-space Green's function for the operator (2) is given by

$$G(r,r',\xi-\xi')=\frac{1}{2\pi}\int_0^{\pi}\cos m\psi\frac{e^{-i\kappa R}}{R}d\psi \quad , \quad (4)$$

where

$$R=\sqrt{r^2+r'^2-2rr'\cos\psi+(\xi-\xi')^2} \quad . \quad (5)$$

Assume that the inlet plane is located at the axial position $\xi=\xi_{in}$ and that the modal functions P^m and $\frac{\partial P^m}{\partial\xi}$ are known on the inlet disc and are zero everywhere else on the inlet plane. Then using the Helmholtz integral representation, we can write the acoustic pressure anywhere in the sound field as[11]

$$P^m(r,\xi)=-\int_0^1 r'\frac{\partial P^m}{\partial\xi'}(r',\xi_{in})G(r,r',\xi-\xi_{in})dr'\pm \int_0^1 r'P^m(r',\xi_{in})\frac{\partial G}{\partial\xi'}(r,r',\xi-\xi_{in})dr' \quad . \quad (6)$$

The positive sign in (6) applies to $\xi>\xi_{in}$ and the negative sign to $\xi<\xi_{in}$.

Evaluation of (6) is simplified considerably if predictions for $\xi<\xi_{in}$ are not desired. For this situation, we set

$$P^m(r,\xi)=0 \qquad \xi<\xi_{in} \quad (7)$$

in (6) yielding the result

$$P^m(r,\xi)= 2\int_0^1 r'P^m(r',\xi_{in})\frac{\partial G}{\partial\xi'}(r,r',\xi-\xi_{in})dr' \qquad \xi>\xi_{in} \quad . \quad (8)$$

Thus, only the acoustic pressure at the inlet is required to compute the forward radiation field.

Denote the axial coordinate of the duct trailing edge by ξ_{ex} and apply the same procedure to the exhaust plane, then we obtain the composite function

$$P^m(r,\xi)= \begin{cases} 0 & \xi\in(\xi_{ex},\xi_{in}) \\ 2\int_0^1 r'P^m(r',\xi_{in})\frac{\partial G}{\partial\xi'}(r,r',\xi-\xi_{in})dr' & \xi>\xi_{in} \\ -2\int_0^1 r'P^m(r',\xi_{ex})\frac{\partial G}{\partial\xi'}(r,r',\xi-\xi_{ex})dr' & \xi<\xi_{ex} \end{cases} \quad (9)$$

for the modal coefficient of acoustic pressure.

Equation (9) extends the classical Rayleigh formula. It includes radiation from the inlet and exhaust planes and is valid for uniform axial inflow.

In practice, Rayleigh's formula is usually applied to a single radial mode obtained from infinite duct theory. We assess the accuracy of this noise prediction technique by comparing radiation patterns computed using (9) with single radial mode input to those generated by TBIEM3D.

Results

In all calculations the duct radius and length are one meter. Incident sound is generated by a circular array of twenty spinning axial dipole point sources. The source disc is perpendicular to the duct axis and located in the middle of the duct. This configuration simulates the thrust component of loading noise generated by a fan with twenty blades. The rotational speed of the source disc is chosen so that only one radial mode is cut-on.

In this study, we compare the radiated field from TBIEM3D with that obtained from (9) with single radial mode input. Two cases are examined, one with no inflow and the other with axial inflow Mach number $M = 0.4$. The rotational speed and source strengths of the dipoles are kept constant for the two cases. In order to obtain a proper comparison between the two methods, the amplitude of the single radial mode must be adjusted to match the TBIEM3D results. This is accomplished by a procedure described in Part II of this paper.

In figure 1 the no inflow case is considered. We plot contours of sound pressure level for the $m = 20$ circumferential coefficient of acoustic pressure in the r-Z plane. Figure 1a shows the field calculated using Rayleigh's formula. TBIEM3D results are displayed in

figure 1b. The radiated patterns for the two cases are very similar in the peak noise region in both direction and amplitude.

Figure 2 contains equivalent results for the $M = 0.4$ case. Again the agreement between the methods is excellent in the peak noise region both forward and aft.

Since edge effects are ignored, details of the complicated diffraction pattern observed in the TBIEM3D results are not captured by the Rayleigh formula predictions.

Discussion

Rayleigh's formula is simple to evaluate and involves little computational effort to produce the radiated field. For the single propagating mode case, the formula provides an excellent noise prediction tool in the peak noise region provided both the reflected and transmitted amplitudes of the mode are known. These quantities are not always available, but for many situations reflection can be ignored and the field accurately calculated with just the transmitted portion of the radial mode.

Since the input function for Rayleigh's formula can have an arbitrary radial distribution, (9) can also be used if more than one mode is propagating. One must then know all modal amplitudes.

TBIEM3D does not explicitly resort to the radial decomposition of the pressure field inside the duct. In fact, near the duct edges the actual pressure field cannot be written as a sum of radial modes in the conventional sense. This is because of the complicated diffraction pattern caused by the sharp duct edges. These effects are accounted for implicitly by TBIEM3D and ignored by the Rayleigh formula representation. Thus, if fine scale details of the radiated field are required, then TBIEM3D would be the prediction method of choice.

Part II: Generalized Radiation Impedance

Theory

The calculation of generalized radiation impedances requires knowledge of the acoustic pressure and acoustic velocity at the inlet. In this work, these quantities have been calculated by TBIEM3D.

The concept of generalized radiation impedance is based on classical infinite duct, spinning mode representations of the acoustic pressure and velocity fields inside the duct. The *m-th* circumferential mode of acoustic pressure inside the duct has the form

$$p^m(r,\psi,Z,t) = P^m(r,Z)e^{i\left(kt - m\psi - \frac{\kappa M}{\beta}Z\right)}, \quad (10a)$$

where

$$P^m(r,Z) = \sum_{n=0}^{\infty}\left(A_{mn}^- e^{-i\kappa_{mn}Z} + A_{mn}^+ e^{+i\kappa_{mn}Z}\right)J_m(\nu_{mn}r), \quad (10b)$$

and $A_{mn}^{\pm}$ are as yet undetermined constants. Note that the summation in (10b) begins at $n = 1$ if $m \neq 0$.

The axial component of acoustic velocity is related to the acoustic pressure via the acoustic momentum equation

$$iku_Z^m - M\frac{\partial u_Z^m}{\partial Z} + \frac{\partial p^m}{\partial Z} = 0 \quad . \quad (11)$$

Using (10-11) u_Z^m can be written as

$$u_Z^m(r,\psi,Z,t) = U_Z^m(r,Z)e^{i\left(kt - m\psi - \frac{\kappa M}{\beta}Z\right)} \quad (12a)$$

with

$$U_Z^m(r,Z) = \sum_{n=0}^{\infty}\left(\mu_{mn}^- A_{mn}^- e^{-i\kappa_{mn}Z} + \mu_{mn}^+ A_{mn}^+ e^{+i\kappa_{mn}Z}\right)J_m(\nu_{mn}r) \quad (12b)$$

and

$$\mu_{mn}^{\pm} = \frac{\beta\kappa_{mn} \mp M\kappa}{\beta M\kappa_{mn} \mp \kappa}. \quad (13)$$

The expansion (10) is not valid near the open ends of a finite length duct. This is because of the singular behavior of the acoustic pressure at the leading and trailing edges[2]. However, the acoustic pressure can be adequately represented by (10) for regions of space inside the duct that are sufficiently far from the ends,.

TBIEM3D does not explicitly calculate the expansion (10). The axial coefficients $A_{mn}^{\pm}$ can be determined by calculating the acoustic pressure on several discs inside the duct. Hankel transforms are calculated for each disc to determine the strengths of the radial modes. The axial coefficients are then obtained by applying a least squares process to the Hankel transform results. Finally the axial component of acoustic velocity inside the duct is determined from (12-13).

Inlet Impedance

For the *m-th* circumferential mode, we define inlet impedance, ζ^m, by the ratio of acoustic pressure to axial velocity evaluated at the inlet. It is evident from

(10) and (12) that ζ^m is a function of the radial variable only.

Assume that the inlet disc is located at $Z=0$ and define the quantities P_n^m and U_n^m by

$$P_n^m = A_{mn}^- + A_{mn}^+ \tag{14}$$

and

$$U_n^m = \mu_{mn}^- A_{mn}^- + \mu_{mn}^+ A_{mn}^+ \quad . \tag{15}$$

These known quantities are related through the inlet impedance, i.e.,

$$\sum_{n=0}^{\infty}\left[P_n^m - U_n^m \zeta^m(r)\right] J_m(\nu_{mn} r) = 0 \quad . \tag{16}$$

The generalized impedances, ζ_{nl}^m are obtained by applying the orthogonality relation[12]

$$\int_0^1 r J_m(\nu_{ml} r) J_m(\nu_{mn} r)\,dr = \frac{1}{2}\left(1 - \frac{m^2}{\nu_{mn}^2}\right) J_m^2(\nu_{mn})\,\delta_{ln} \quad , \tag{17}$$

where δ_{ln} is the Kronecker delta, to (16). This yields the result

$$P_n^m = \sum_{l=0}^{\infty} \zeta_{nl}^m U_l^m \quad , \tag{18}$$

where the generalized radiation impedances are given by the formula

$$\zeta_{nl}^m = \frac{2\nu_{mn}^2}{\left(\nu_{mn}^2 - m^2\right) J_m^2(\nu_{mn})} \times \int_0^1 r \zeta^m(r) J_m(\nu_{ml} r) J_m(\nu_{mn} r)\,dr \quad . \tag{19}$$

Acoustic Power Transmission Coefficient

The acoustic power radiated from the inlet due to the *m-th* circumferential mode is obtained by integrating the axial component of the acoustic intensity vector over the inlet disc.

At any location inside the duct, the axial component of intensity can be written as

$$I_Z^m = \frac{1}{2} Re\left\{\left(P^m - M U_Z^m\right)\left(U_Z^m - M P^m\right)^*\right\} \quad . \tag{20}$$

In (20), the asterisk superscript denotes the complex conjugate. Evaluating the axial intensity at the inlet yields

$$I_Z^m\big|_{inlet} = \frac{1}{2}\left|U_Z^m\right|^2 Re\left\{\left(\zeta^m - M\right)\left(1 - M\zeta^m\right)^*\right\} \quad . \tag{21}$$

The power radiation analysis that follows will be considered for individual radial modes. Using the axial coefficients obtained from TBIEM3D above, we write the acoustic pressure and axial velocity for a single radial mode as

$$P^m(r,Z) = A_{mn}^-\left(e^{-i\kappa_{mn}Z} + R_n^m e^{+i\kappa_{mn}Z}\right) J_m(\nu_{mn} r) \quad , \tag{22}$$

and

$$U_Z^m(r,Z) = A_{mn}^-\left(\mu_{mn}^- e^{-i\kappa_{mn}Z} + \mu_{mn}^+ R_n^m e^{+i\kappa_{mn}Z}\right) J_m(\nu_{mn} r) \quad , \tag{23}$$

where the pressure reflection coefficients, R_n^m, are given by

$$R_n^m = \frac{A_{mn}^+}{A_{mn}^-} \tag{24}$$

and account for reflection from the duct inlet.

The inlet impedance for this situation is constant and given by

$$\zeta^m = \frac{1 + R_n^m}{\mu_{nm}^- + \mu_{nm}^+ R_n^m} \quad . \tag{25}$$

Using (22-25), we write the axial intensity at the inlet in terms of the inlet impedance. Thus,

$$I_Z^m\big|_{inlet} = \frac{1}{2}\left|A_{mn}^- J_m(\nu_{mn} r)\right|^2 \left|\mu_{mn}^- + \mu_{mn}^+ R_n^m\right|^2 \times Re\left\{\left(\zeta^m - M\right)\left(1 - M\zeta^m\right)^*\right\} \quad . \tag{26}$$

We are also interested in the axial intensity at the inlet due to the incident wave only which we denote by $\left(I_Z^m\right)_{inc}\big|_{inlet}$. This is obtained from (26) by setting $R_n^m = 0$. Therefore,

$$\left(I_Z^m\right)_{inc}\big|_{inlet} = \frac{1}{2}\left|A_{mn}^- J_m(\nu_{mn} r)\right|^2 \times Re\left\{\left(1 - M\mu_{mn}^-\right)\left(\mu_{mn}^- - M\right)^*\right\} \quad . \tag{27}$$

Define the acoustic power transmission coefficient for the *(m,n)* mode, Π_n^m, as the ratio of power transmitted through the inlet disc to incident power through the disc. For the case considered here, this quantity is simply the ratio of axial intensities at the inlet which yields the result

$$\Pi_n^m = \left|\mu_{mn}^- + \mu_{mn}^+ R_n^m\right|^2 \times \frac{Re\left\{\left(\zeta^m - M\right)\left(1 - M\zeta^m\right)^*\right\}}{Re\left\{\left(1 - M\mu_{mn}^-\right)\left(\mu_{mn}^- - M\right)^*\right\}} \quad . \tag{28}$$

Formula (28) is an alternative but equivalent representation of the power coefficient originally derived by Rice[13].

Results

We illustrate the usefulness of TBIEM3D in computing the generalized radiation impedances and power transmission coefficients by considering a wide range of operating parameters and mode numbers.

In all results the duct radius and length are one meter. Incident sound is generated by a circular array of either spinning or non-spinning axial dipole point sources located just aft of the duct trailing edge. Variations in impedance and power transmission due to duct length and source type were not investigated.

Results are presented for nine cases. Three circumferential mode numbers, $m = 0, 4$, and 10, are considered. For each circumferential mode, we calculate results for three inflow Mach numbers, $M = 0.0, 0.2$, and 0.6. All calculations were performed on a personal computer with a Pentium 133 processor with 32 megabytes of RAM..

In figures 3-5, the real and imaginary parts of the generalized radiation impedances ζ^0_{00}, ζ^0_{10}, and ζ^0_{11} are plotted as functions of κ for the three inflow Mach numbers. Figures 6-8 contain graphs of ζ^4_{11}, ζ^4_{12}, and ζ^4_{22}. The functions ζ^{10}_{11}, ζ^{10}_{12}, and ζ^{10}_{22} are displayed in figures 9-11. Vertical lines in these figures mark the infinite duct cut-off frequencies.

The power transmission coefficients Π^0_0, Π^0_1, and Π^0_2 are plotted as functions of κ in figure 12 for each Mach number case. Figures 13 and 14 display similar results for the $m = 4$ and $m = 10$ cases, respectively.

Discussion

Several researchers have studied modal impedances and power transmission at cylindrical duct terminations (e.g., refs. 3-8). In references 3-5, impedance calculations were based on Rayleigh's formula. Later research such as that in references 6-8 employed more precise boundary element or Wiener-Hopf noise prediction methods. The highest circumferential mode order for which calculated results were presented was $m = 3$.

The results shown here for $m = 0$ and $m = 4$ agree qualitatively with those earlier results. Specifically, the direct impedances, ζ^m_{nn}, all approach $1 + 0i$ for increasing κ. Most discontinuities in the impedance curves occur at or near the cut-on frequencies of higher order radial modes. Except for the M = 0.6 case, the associated power transmission coefficients approach unity fairly quickly once the mode is cut on.

For $M = 0.0$ and 0.2, the cross-modal impedances ζ^0_{01} and ζ^m_{12} in figures 3, 4, 6, 7, 9, and 10, are nonzero for smaller values of κ and slowly tend to zero for large κ. For $M = 0.6$, intermodal coupling is quite weak for all values of κ as evidenced by the results in figures 5, 8, and 11. These observations reinforce the intuitive concept that cross-coupling between radial modes should be relatively weak except when one of the modes is just above its cut-on frequency.

Trends in the computed results are most clearly identified by examining the power transmission coefficients in figures 12-14. For example, there is little change in the transmission coefficients for the $m = 0$ and 4 cases as M increases from 0.0 to 0.2. Figures 12c, 13c, and 14c indicate reduced modal transmission as higher order radial modes are cut on. This effect is enhanced for larger order circumferential modes.

As the circumferential mode order m and inflow Mach number M increase, the generalized radiation impedance and power transmission curves become more oscillatory. The reasons for these phenomena are not fully understood and require further study.

Johnston and Ogimoto (ref. 7), noted considerable influence of duct length on the radiation impedances. This is absent in our calculations because of the shortness of the duct examined. In reference 7, a duct length of 10 radii was used, while the current study considers a duct length of one radius. The short duct greatly weakens the organ pipe resonance phenomenon responsible for the duct length effects observed in reference 7.

Concluding Remarks

We have examined two aspects of duct propagation and radiation which can contribute to more efficient fan noise predictions. Rayleigh's formula was expanded to include uniform axial inflow. Forward and aft radiation can be computed using equation (9). Comparisons with TBIEM3D results shows that Rayleigh's formula with single radial mode input accurately predicts sound directivity and levels in the peak noise regions both forward and aft.

The ducted fan noise prediction code TBIEM3D was used to calculate modal impedances and transmission coefficients for a wide range of operating parameters. Results were obtained for higher Mach numbers and circumferential mode orders than has been previously published. Due to their simplicity and ease of use, both of these tools should be of value to the engine nacelle designer.

Acknowledgement

The authors gratefully acknowledge insightful technical discussions on this research held with Dr. Edward J. Rice and Dr. William E. Zorumski.

References

1. M.H. Dunn: TBIEM3D – A Computer Program for Predicting Ducted Fan Engine Noise, Version 1.1. NASA/CR-97-206232, September 1997.

2. M.H. Dunn, J. Tweed, and F. Farassat: The Prediction of Ducted Fan Engine Noise Via a Boundary Integral Equation Method. AIAA Paper 96-1770, April, 1996.

3. C.L. Morfey: A Note on the Radiation Efficiency of Acoustic Duct Modes. J. Sound and Vibration, Vol. 9, p 367-372, 1969.

4. William E. Zorumski: Generalized Radiation Impedances and Reflection Coefficients of Circular and Annular Ducts. J. Acoust. Soc. Am, Vol. 54, p 1667-1673, 1973.

5. Edward J. Rice: Multimodal Far-Field Acoustic Radiation Pattern Using Mode Cut-off Ratio. AIAA Journal, Vol. 16, p 906-911, 1978.

6. K. Ogimoto and G.W. Johnson: Modal Radiation Impedances for Semi-Infinite Unflanged Circular Ducts Including Flow Effects. J. of Sound and Vibration, Vol. 62, p 598-605, 1979.

7. G.W. Johnson and K. Ogimoto: Sound Radiation from a Finite Length Unflanged Circular Duct with Uniform Axial Inflow. II. Computed Radiation Characteristics. J. Acoust. Soc. Am., Vol. 68, p 1871-1883, 1980.

8. K.S. Wang and T.C Tszeng: Propagation and Radiation of Sound in a Finite Length Duct. J. of Sound and Vibration, Vol. 93, p 57-79, 1984.

9. Allan D. Pierce: Acoustics - An Introduction to its Physical Principals and Applications. Acoustical Society of America, 1989.

10. J.M. Tyler and T.G. Sofrin: Axial Flow Compressor Noise Studies. SAE Transactions, Vol. 70, p 309-332, 1962.

11. V.I. Smirnov: A Course of Higher Mathematics. Vol. IV, Pergamon Press, Oxford, 1964.

12. G.N. Watson: A Treatise on the Theory of Bessel Functions, Second Edition. Cambridge University Press, Cambridge, England, 1962.

13. Edward J. Rice: Personal Communication.

a) Rayleigh's Formula

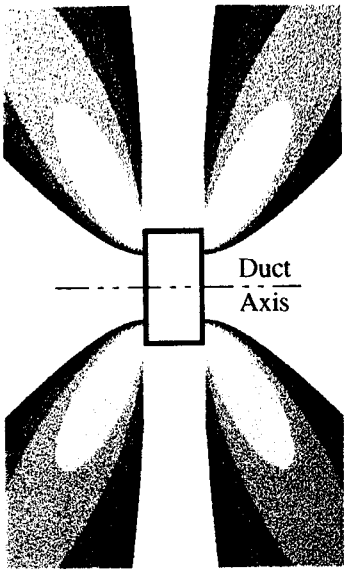

b) TBIEM3D

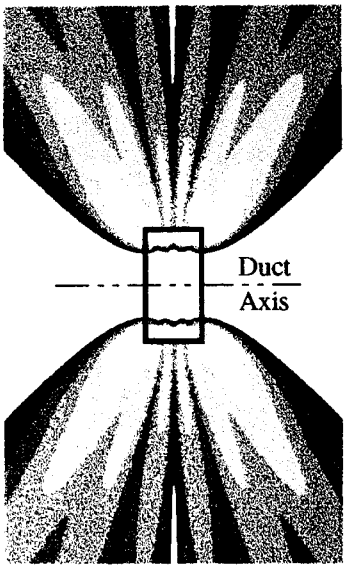

Figure 1: Comparison Between Rayleigh's Formula and TBIEM3D
M = 0.0 m = 20 κ = 25.0

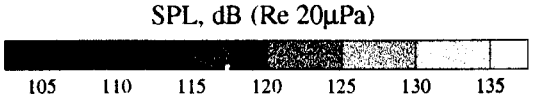

a) Rayleigh's Formula

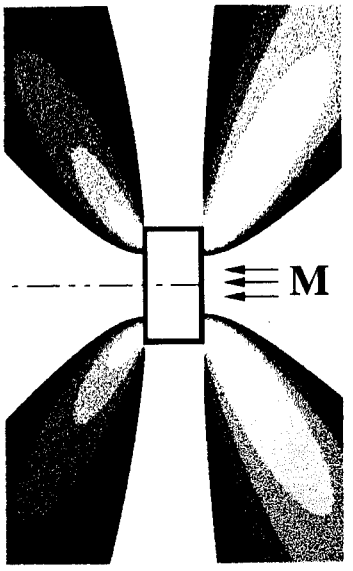

b) TBIEM3D

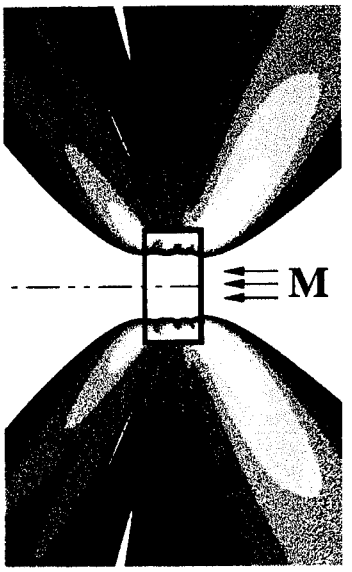

Figure 2: Comparison Between Rayleigh's Formula and TBIEM3D
M = 0.4 m = 20 κ = 27.3

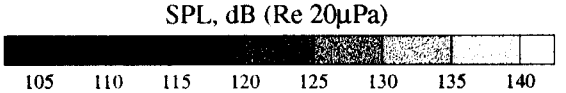

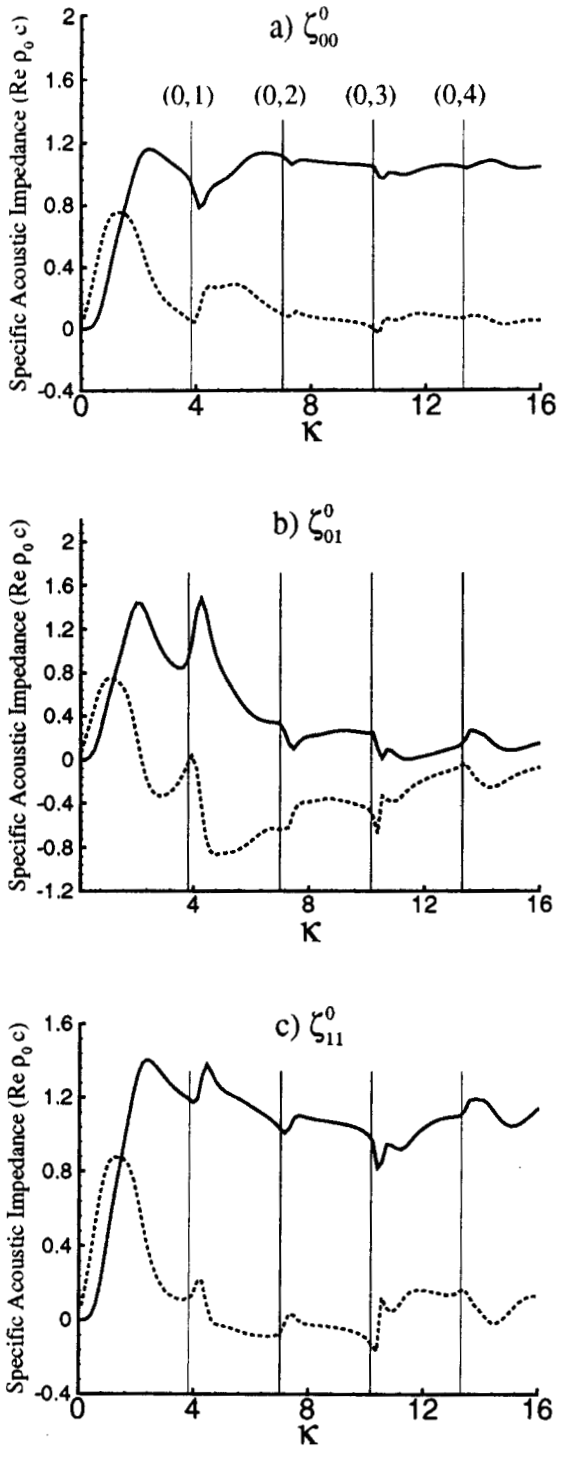

Figure 3: Generalized Radiation Impedance
m = 0 M = 0.0
Resistance
Reactance

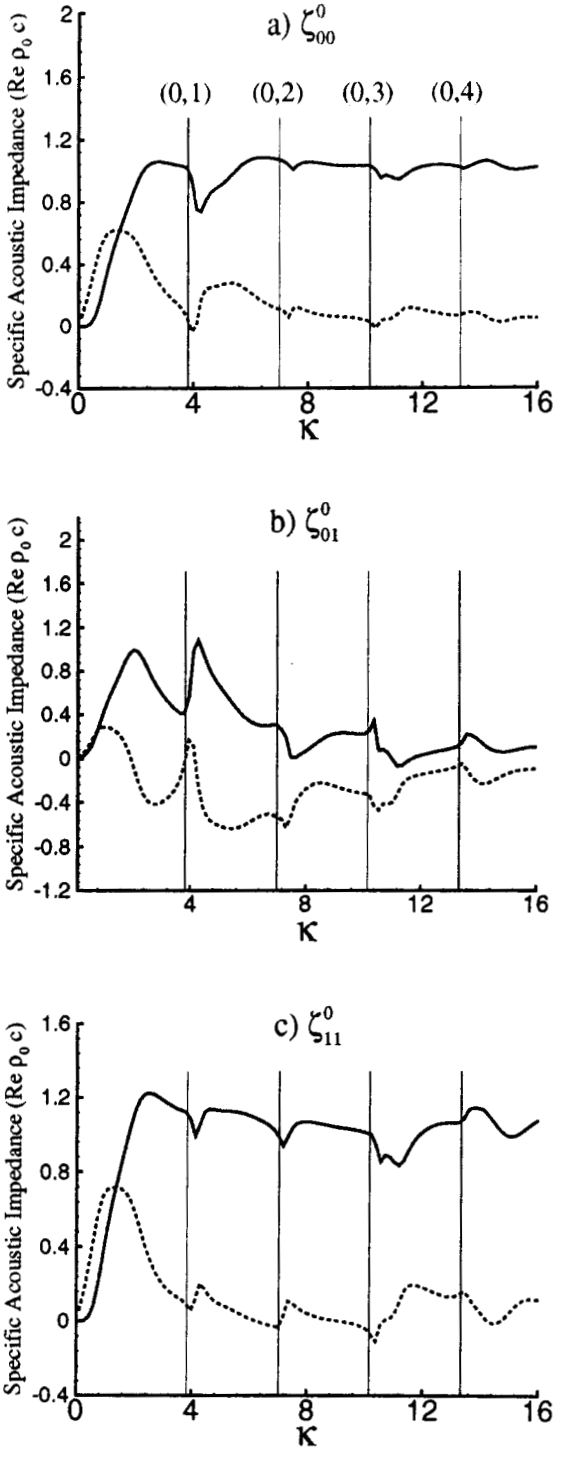

Figure 4: Generalized Radiation Impedance
m = 0 M = 0.2
Resistance
Reactance

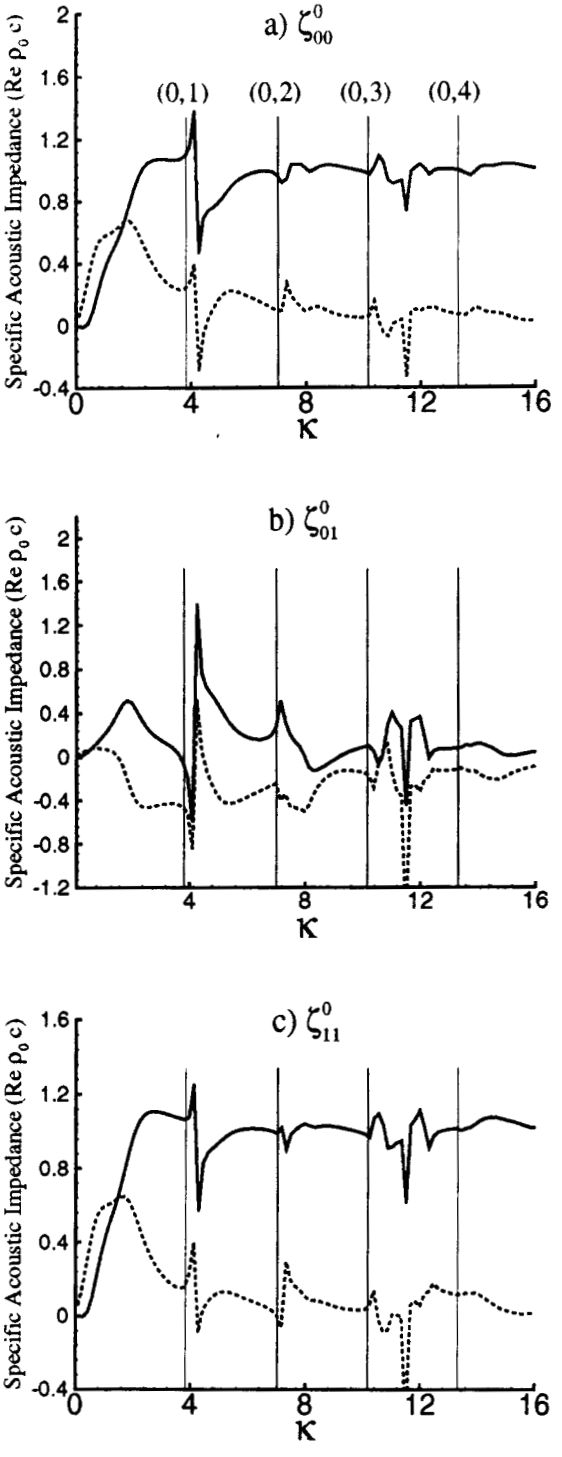

Figure 5: Generalized Radiation Impedance
m = 0 M = 0.6
Resistance
Reactance

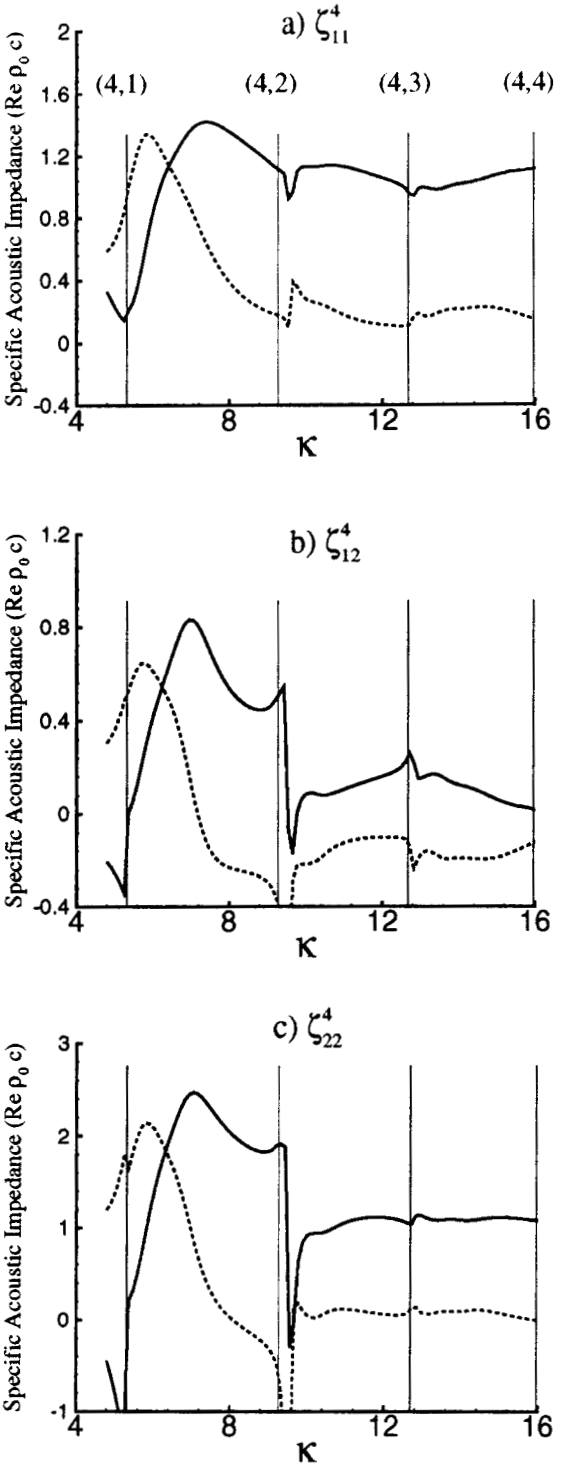

Figure 6: Generalized Radiation Impedance
m = 4 M = 0.0
Resistance
Reactance

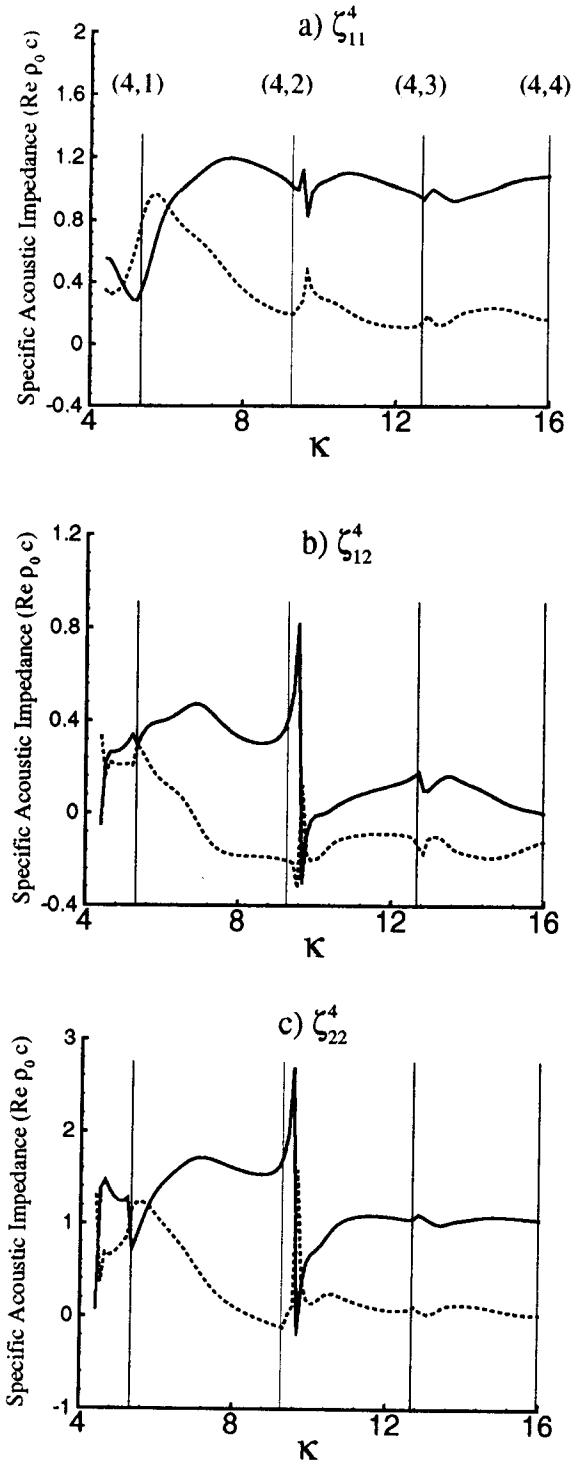

Figure 7: Generalized Radiation Impedance
m = 4 M = 0.2

Resistance

Reactance

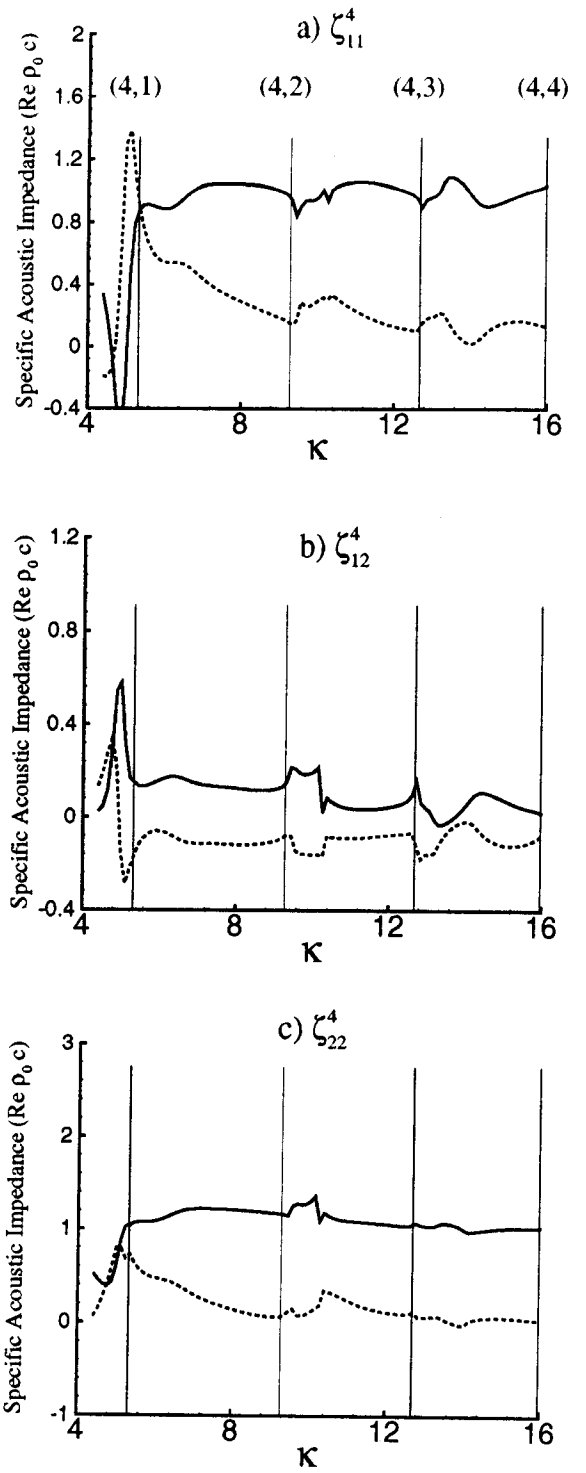

Figure 8: Generalized Radiation Impedance
m = 4 M = 0.6

Resistance

Reactance

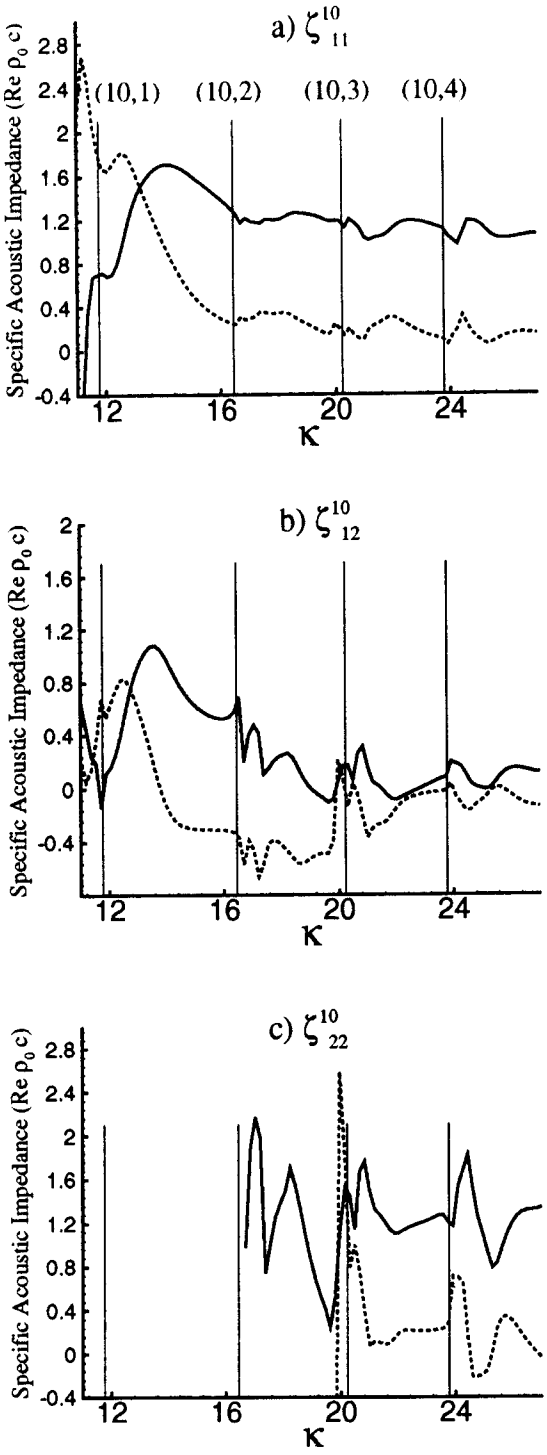

Figure 9: Generalized Radiation Impedance
m = 10 M = 0.0

——— Resistance
..... Reactance

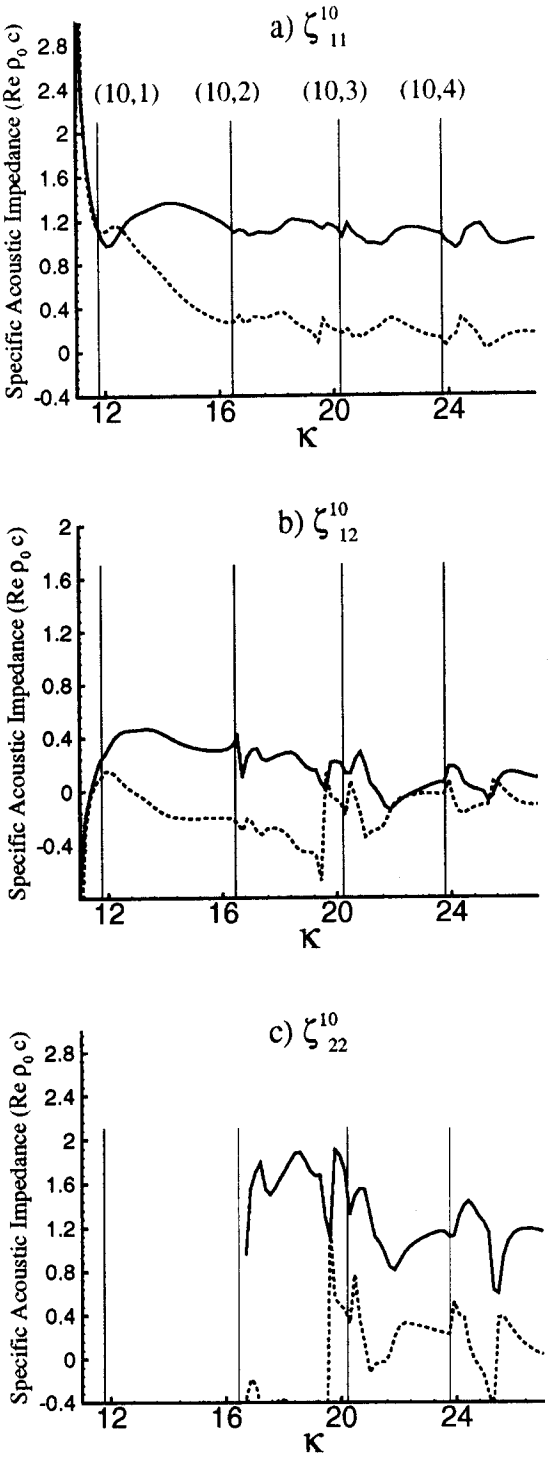

Figure 10: Generalized Radiation Impedance
m = 10 M = 0.2

——— Resistance
..... Reactance

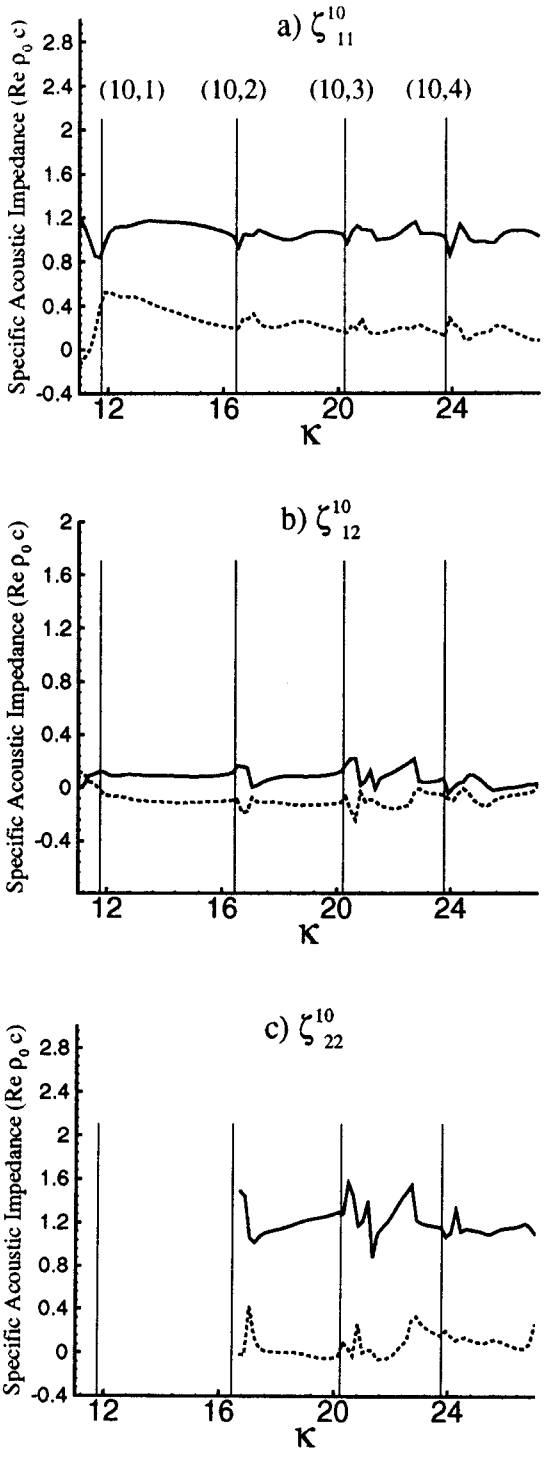

Figure 11: Generalized Radiation Impedance
m = 10 M = 0.6

——— Resistance
····· Reactance

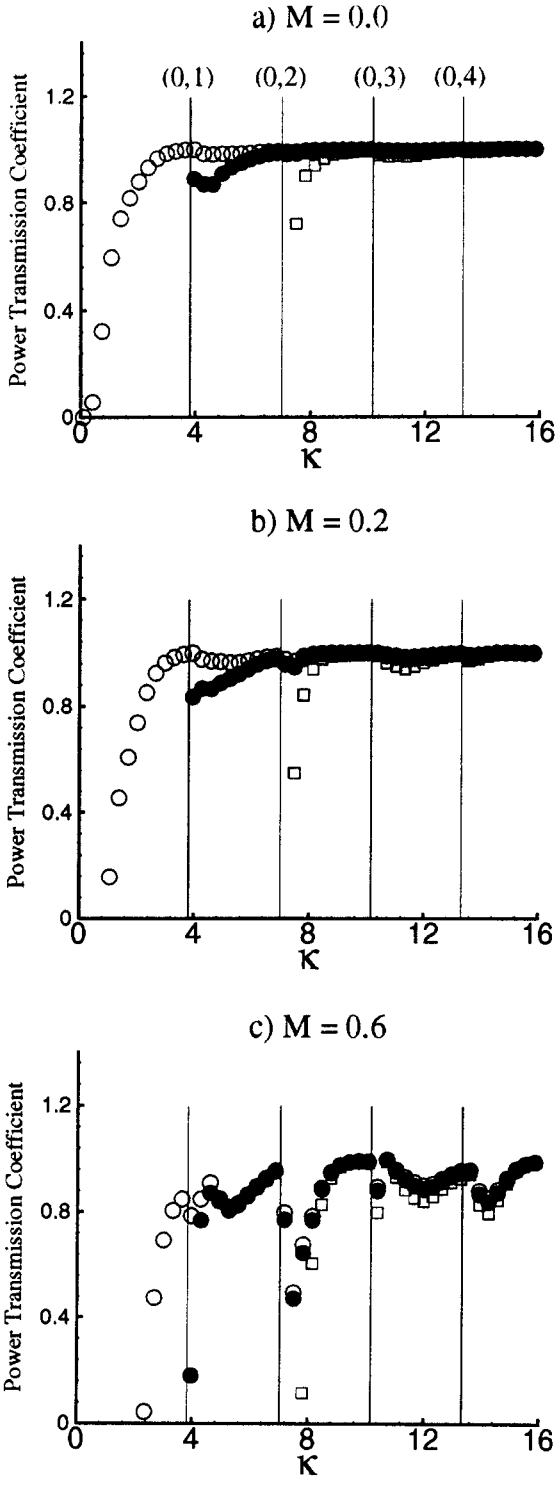

Figure 12: Power Transmission Coefficient: m = 0

○ Π^0_0 ● Π^0_1 □ Π^0_2

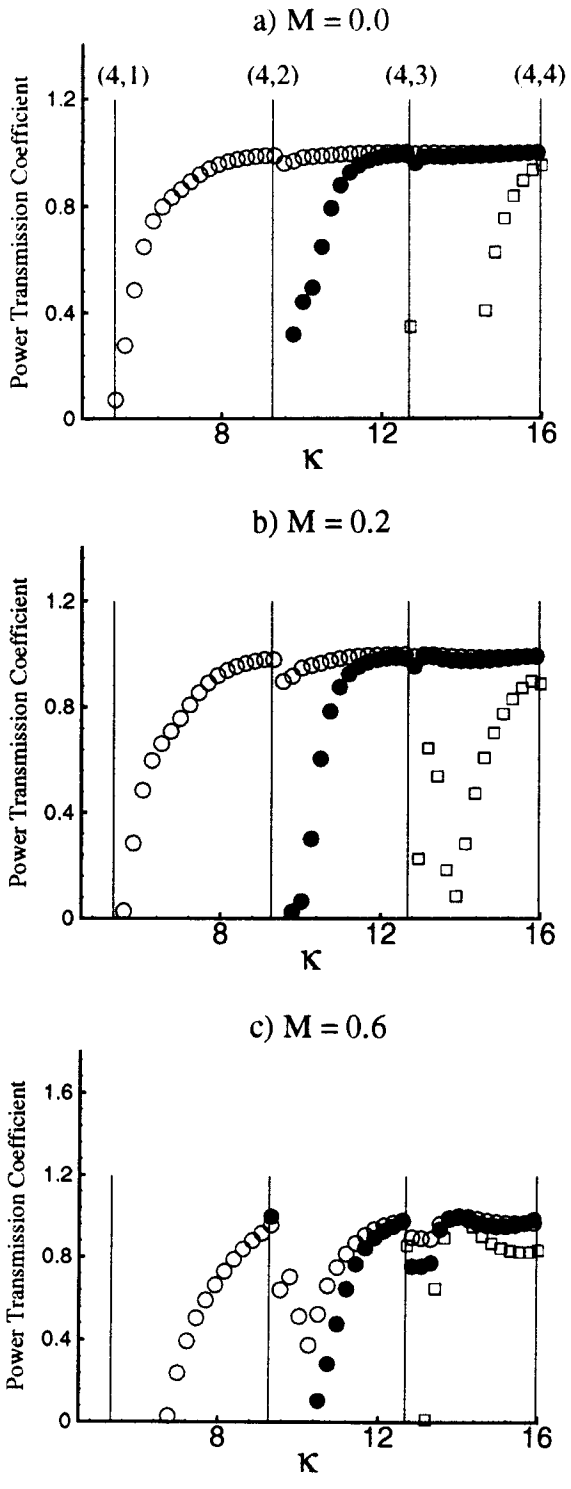

Figure 13: Power Transmission Coefficient: m = 4

○ Π_1^4 ● Π_2^4 □ Π_3^4

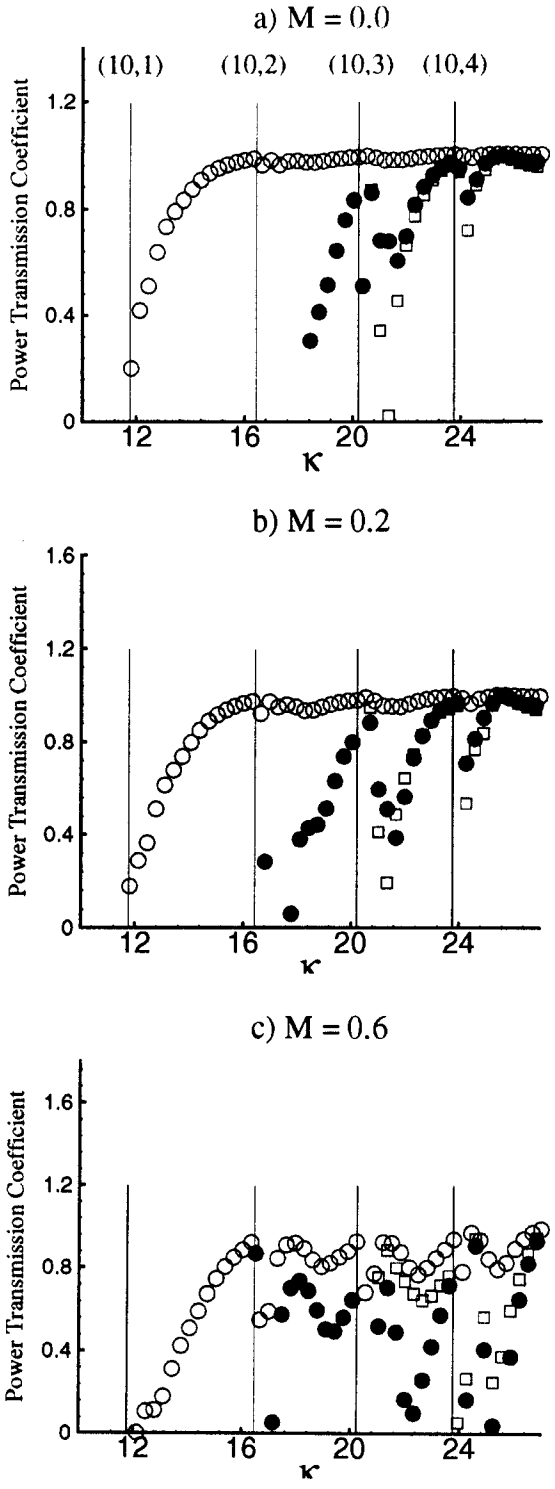

Figure 14: Power Transmission Coefficient: m = 10

○ Π_1^{10} ● Π_2^{10} □ Π_3^{10}